nature neuroscience

Nonlinear dendritic integration of electrical and chemical synaptic inputs drives fine-scale correlations

Stuart Trenholm[1,5,6], Amanda J McLaughlin[1,6], David J Schwab[2], Maxwell H Turner[3], Robert G Smith[4], Fred Rieke[3] & Gautam B Awatramani[1]

Throughout the CNS, gap junction–mediated electrical signals synchronize neural activity on millisecond timescales via cooperative interactions with chemical synapses. However, gap junction–mediated synchrony has rarely been studied in the context of varying spatiotemporal patterns of electrical and chemical synaptic activity. Thus, the mechanism underlying fine-scale synchrony and its relationship to neural coding remain unclear. We examined spike synchrony in pairs of genetically identified, electrically coupled ganglion cells in mouse retina. We found that coincident electrical and chemical synaptic inputs, but not electrical inputs alone, elicited synchronized dendritic spikes in subregions of coupled dendritic trees. The resulting nonlinear integration produced fine-scale synchrony in the cells' spike output, specifically for light stimuli driving input to the regions of dendritic overlap. In addition, the strength of synchrony varied inversely with spike rate. Together, these features may allow synchronized activity to encode information about the spatial distribution of light that is ambiguous on the basis of spike rate alone.

Gap junctions between neurons convey electrical signals with high temporal precision and fidelity, permitting action potentials in electrically coupled neurons, for brief instances, to influence the spiking behavior of their neighbors, giving rise to fine-scale synchrony (reviewed in refs. 1 and 2). However, in many areas of the brain, including the retina[3], cortex[4], inferior olive[5], hippocampus[6], locus coeruleus[7], cochlear nucleus[8], olfactory bulb[9] and cerebellum[10,11], gap junctions are found at distal dendritic locations and typically have small unitary conductances[1,2]. When action potentials back-propagating into distal dendrites traverse high-resistance gap junctions and feed into the parallel capacitive and resistive elements of post-junctional cells, they are low-pass filtered and highly attenuated, giving rise to small-amplitude coupled spikelets (~1 mV) at the somata of post-junctional neurons[1,2]. The relatively small amplitude of coupled spikelets compared with chemical synaptic inputs has made it difficult to understand how electrical signals can synchronize spike output between neighboring neurons under natural stimulation conditions[12].

Recent work has shown that gap junctions found at distal dendritic sites can interact locally with chemical synaptic inputs to enrich the computational abilities of neural circuits[10,11,13–18]. In one elegant study, in which two-photon glutamate uncaging techniques were used to simulate chemical synaptic inputs, it was found that gap junction inputs could compensate for sublinear synaptic integration in the passive dendrites of cerebellar Golgi interneurons[15]. However, in neurons with active dendrites, theoretical considerations suggest that electrical and chemical synaptic interactions can produce more complex features, such as spike synchrony[19,20]. Nonetheless, it is difficult to experimentally verify the role of electrical and chemical synaptic interactions in driving synchrony, as this would involve recording responses from pairs of neighboring coupled neurons while stimulating the intact network with different naturalistic spatiotemporal patterns of synaptic activity.

To understand the biophysical mechanisms underlying fine scale synchrony, we measured spike trains in pairs of neighboring superior-coding ON-OFF directionally selective retinal ganglion cells (RGCs) labeled in the transgenic *Hb9::eGFP* mouse retina[21], which we have previously shown to be electrically coupled[13,14] (we henceforth refer to these cells as cRGCs). By projecting simple patterns of light stimuli onto the array of photoreceptors in an intact *in vitro* whole-mount retinal preparation, we controlled the activation of synaptic inputs to the planar dendrites of cRGCs, which stratify in distinct layers in the inner retina. Using a combined two-photon imaging, genetic, electrophysiological and pharmacological approach, we found a role for active dendrites in driving gap junction–mediated fine-scale correlations. We also discovered how synchrony can encode information about the spatial distribution of light that is absent from the spike rate.

RESULTS

Gap junctions are required for fine-scale synchrony

Previous work has shown that correlated spike activity between neighboring RGCs occurs on multiple timescales (~1–100 ms) depending on its precise origin[22,23]. We computed cross-correlograms from light-evoked spike trains measured simultaneously in pairs of neighboring cRGCs (**Fig. 1a–d**) and found bimodal peaks within a ±2-ms delay, characteristic of fine-scale synchrony mediated by reciprocal gap junction connectivity[20,24–27]. The two peaks in the cross-correlogram were

[1]Department of Biology, University of Victoria, Victoria, British Columbia, Canada. [2]Department of Physics, Princeton University, Princeton, New Jersey, USA. [3]Department of Physiology and Biophysics, University of Washington, Seattle, Washington, USA. [4]Department of Neuroscience, University of Pennsylvania, Philadelphia, Pennsylvania, USA. [5]Present address: Department of Neurobiology, Friedrich Miescher Institute, Basel, Switzerland. [6]These authors contributed equally to this work. Correspondence should be addressed to G.B.A. (gautam@uvic.ca).

Received 18 August; accepted 1 October; published online 26 October 2014; doi:10.1038/nn.3851

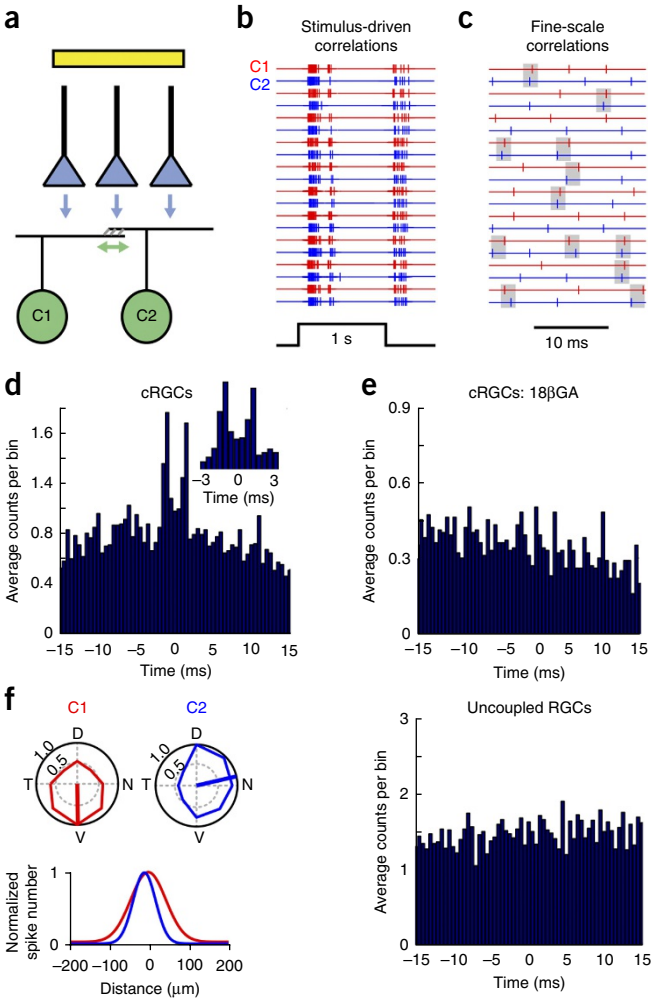

Figure 1 Gap junctions between ganglion cells mediate fine-scale correlated activity. (**a**) A cartoon cross-section of the inner retina, depicting glutamatergic bipolar cells terminals (blue triangles) synapsing onto electrically coupled RGCs, labeled in the *Hb9::eGFP* retina (green cells; for simplicity only the ON dendrites are drawn). The flash used to stimulate the photoreceptors (not shown) is illustrated by the yellow bar. The vertical and horizontal arrows indicate chemical and reciprocal electrical synapses, respectively. (**b**) Spike trains evoked by a high-contrast spot (300-μm diameter, 10 trials), measured simultaneously from a pair of neighboring cRGCs (C1 and C2), are synchronized on a broad timescale by the stimulus. (**c**) A high temporal resolution view of a portion of the ON response shown in **b** illustrates fine-scale correlated spikes (highlighted by gray boxes, 2 ms) that are independent of the stimulus. (**d**) A cross-correlogram that indicates the distribution of spike times measured in C2 relative to each spike in C1 (0.5-ms bins). Inset shows the fine-scale correlated peaks in the cross-correlogram at higher temporal resolution. (**e**) The bimodal peaks (within ±2 ms) in the cross-correlogram were abolished in the presence of the gap junction blocker 18βGA (25 μM). Correlations were also weaker between $Hb9^+$ cells in *Cx36*$^{-/-}$ retina (**Supplementary Fig. 5**). (**f**) Polar plots (top left) indicating the peak spike rate (normalized to the preferred direction) evoked by stimuli moving in eight directions, measured simultaneously in a pair of uncoupled directionally selective ganglion cells (C1 and C2) coding different directions. Gaussian approximations of their receptive fields, indicating the high degree of receptive field overlap between C1 and C2 (bottom left, Online Methods). Right, cross-correlogram for light-evoked spike activity for this pair of uncoupled RGCs. D, dorsal; N, nasal; V, ventral; T, temporal.

not always of the same amplitude, but could easily be separated from broader stimulus-driven correlations using a shift predictor computed from shuffled trials (**Supplementary Fig. 1**). The strength of fine-scale correlations was quantified using a correlation index (CI, larger values indicate stronger correlations, Online Methods). For spike trains evoked by drifting gratings, the CI was found to be 0.13 ± 0.03 (n = 8 pairs; given that spike correlations were present for both ON and OFF responses to a flash of light, these components were combined for analysis; **Supplementary Fig. 2**).

Fine-scale spike correlations between cRGCs were weak or absent in the presence of the gap junction blocker 18β-glycyrrhetinic acid[13,14,28] (18βGA, 25 μM, CI = 0.05 ± 0.01, n = 6 pairs, $P < 0.0001$, $t_5 = 6.756$, paired t test; **Fig. 1e**; 18βGA had only a minor effect on the light response; **Supplementary Fig. 3**) or when measured between pairs of neighboring uncoupled directionally selective RGCs[13] with significant receptive field overlap (CI = 0.06 ± 0.01, n = 5 pairs, P = 0.01, t_{11} = 3.080, t test; **Fig. 1f** and **Supplementary Fig. 4**). As further evidence that gap junctions between cRGCs are required for fine-scale correlations, correlated spiking was reduced in Connexin 36 knockout retina (*Cx36*$^{-/-}$; also known as *Gjd2*), in which coupling between cRGCs was found to be minimal (CI = 0.03 ± 0.01, n = 3 pairs, P = 0.01, t_9 = 3.241; **Supplementary Fig. 5**). Taken together, these results strongly suggest that reciprocal gap junction connections are critically required for the generation of fine-scale spike correlations, supporting previous findings[20,24–27].

Coupled spikelets exert little effect at the soma

In attempting to define the biophysical underpinnings of gap junction–mediated correlations, many studies have relied on *in vitro* brain slice preparations in which circuit properties are not well preserved and somatic current injections are used as a proxy for synaptic activity[1,2]. Indeed, when neighboring cRGCs were simultaneously depolarized through the recording electrode, robust correlations were observed (**Fig. 2a–c**), which persisted in the presence of a cocktail of chemical synaptic blockers (**Supplementary Fig. 6**).

In this scenario, action potentials back-propagate through the dendritic tree of the donor cell, cross the gap junction and give rise to transient ~1-mV coupled spikelets at the soma of the recipient cell, which are revealed occasionally when a post-junctional cell fails to fire an action potential (**Fig. 2b**) or when the pre-junctional, but not post-junctional, cell is directly activated[13]. These small-amplitude coupled spikelets arrive at the post-junctional soma with submillisecond precision and are thought to be the signals that synchronize spike activity[11,29]. However, the relevance of this simplistic experimental procedure and its interpretation are questionable, as they disregard the natural spatiotemporal aspect of synaptic inputs and the active dendritic conductances that are known to be important during physiological activation of many neurons.

To directly test whether coupled spikelets exert a substantial action at the soma, we injected Poisson-distributed trains of brief current pulses through a patch pipette, mimicking gap junction–mediated somatic spikelets arising from trains of action potentials in neighboring cRGCs. We then examined whether these artificial spikelets could alter the timing of light-evoked action potentials measured in the same neuron (**Fig. 2d**). We found that simulated coupled spikelets with a peak amplitude comparable to that of experimentally measured gap junction inputs (~1 mV at the soma) produced no measurable effect on spike timing (**Fig. 2e,f**). However, larger currents producing somatic depolarizations that were in the range of ~5–20 mV in peak amplitude effectively modulated the precise timing of the light-evoked action potentials, generating a fine-scale synchrony similar to

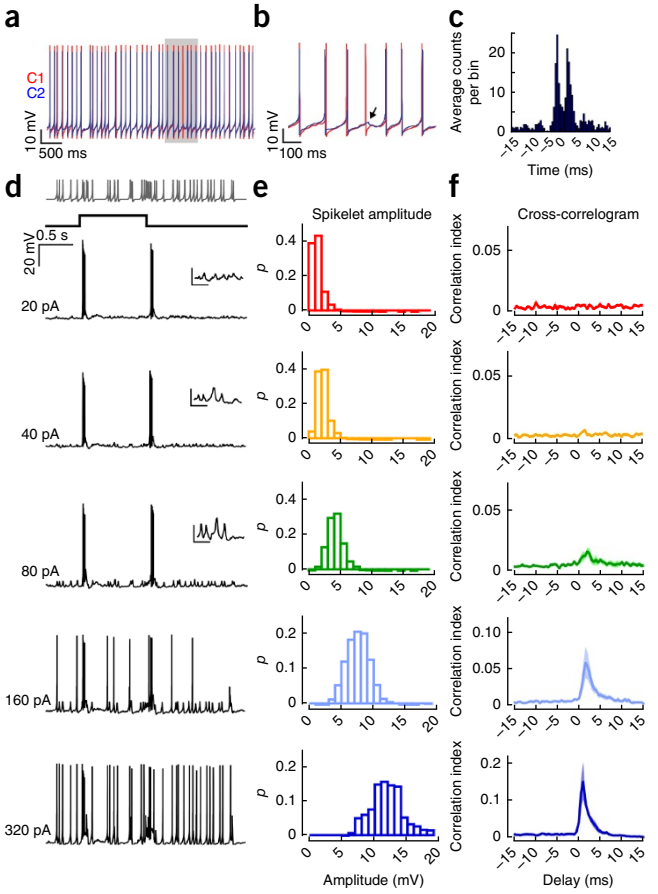

Figure 2 Simulated coupled spikelets do not act at the soma to drive correlated spiking. (**a**) Spiking responses in a pair of cRGCs (C1 red, C2 blue) in which both cells were injected with constant depolarizing current (~200 pA) through the patch electrode. (**b**) The area shaded in gray in **a** is shown at higher temporal resolution. The arrow points to a coupled spikelet (driven by C1) revealed during a spike failure in C2. (**c**) A cross-correlogram computed for spike trains measured in the pair of cRGCs shown in **a**. (**d**) Representative responses of an ON-OFF directionally selective RGC to a 1-s light flash while a Poisson-distributed train of simulated spikelets (indicated on top) of varying amplitudes (indicated on the left) were injected into the soma. The insets show the voltage responses to the spikelet injections at higher magnification (scale bars represent 5 mV, 100 ms). (**e**) Plots of the distribution of peak membrane depolarizations evoked by different-sized current injections. *p* is the fraction of spikelets in each bin. (**f**) CI between injected spikelets and light-evoked action potentials plotted as a function of delay (n = 6 cells).

that measured between neighboring cRGCs (note that the correlation function does not have two peaks because simulated spikelets were injected into only a single cell; **Fig. 2e**,**f**). Thus, we conclude that the synchronization signal must be considerably larger than the ~1-mV coupled spikelets measured at the soma, which were generated exclusively by gap junction inputs (**Fig. 3a**).

Coupled spikelets alone do not drive dendritic spikes

We next considered the possibility that nonlinear dendritic mechanisms might amplify distal gap junction–mediated signals and generate active synchronization signals. First, to test whether the dendrites of cRGCs were active, we stimulated cRGCs with light while preventing the generation of somatic action potentials by either locally applying tetrodotoxin (TTX) over the soma/axon hillock (**Fig. 3b**) or by applying a steady hyperpolarizing current to the soma (**Supplementary Fig. 7**). As previously described for rabbit directionally selective ganglion cells[30,31], dendritic spikes were revealed in mouse cRGCs when somatic action potentials were compromised (**Fig. 3b** and **Supplementary Fig. 7**). These dendritic spikes, measured at the soma, likely originate from different branches of the dendritic tree, as they did not exhibit a clear refractory period[30,31] (**Fig. 3c** and **Supplementary Fig. 7**), allowing them to be differentiated from somatic action potentials. In addition, dendritic spikes were blocked when TTX was applied over the entire dendritic arbour (**Fig. 3b**). Thus, TTX-sensitive dendritic spikes appear to be a conserved feature of directionally selective ganglion cells in both mouse and rabbit retina, suggesting they are important in coding stimulus direction[30,31].

In mouse directionally selective cRGCs, dendritic spikes measured at the soma were further distinguished from both coupled spikelets and somatic action potentials on the basis of amplitude and kinetics (n = 4–6 cells, $P < 0.001$, H(2) = 141.197, Kruskal-Wallis one-way ANOVA on ranks; **Fig. 3d**–**f**). However, given that the manipulations used to reveal distal dendritic spikes (TTX puff application or membrane hyperpolarization) altered the properties of proximal dendrites, the measured amplitude of dendritic spikes likely underrepresents their true amplitude[30]. Nevertheless, the clear separation of the amplitude distributions of coupled spikelets and dendritic spikes indicates that gap junction signals alone never directly evoke dendritic spikes. Thus, we hypothesized that if gap junction inputs and chemical synaptic inputs sum to produce dendritic spikes, these would be effective intermediaries that would allow weak distal gap junction inputs to synchronize somatic action potentials.

Dendritic synchrony

To test whether dendritic spikes were required for spike synchrony, we made paired recordings from cRGCs and puffed TTX (**Fig. 4a**) locally over the region of dendritic overlap between neighboring cRGCs (**Fig. 4b**). We found that dendritic TTX application did not affect the properties of somatic action potentials (**Supplementary Fig. 8**), but significantly reduced the strength of correlations (58 ± 10% reduction in CI, n = 5 pairs, P = 0.017, t_4 = 3.959, paired t test; **Fig. 4b**). Given that local dendritic application of TTX was expected to block forward-propagating dendritic spikes[30,31], it was not surprising that it reduced the light-driven spike rate measured at the soma (P = 0.008, t_4 = 3.365, paired t test). However, we explicitly compared the relationship between correlation strength and spike rate and found that the TTX-induced reduction in spike rate cannot account for the loss of correlations (shown below). Na^+ channels have been shown to boost gap junction signaling in several brain regions[11,32,33]. However, our findings demonstrate an obligatory role for dendritic voltage-dependent Na^+ channels in directly mediating fine-scale synchrony.

If coincident electrical and chemical synaptic inputs are indeed nonlinearly integrated, it is expected that the somatic action potentials that back-propagate to drive gap junction inputs would be synchronized with dendritic spikes of post-junctional neighbors. In lieu of patching the fine dendrites of cRGCs, which is technically difficult and could disturb the local circuitry at the recording site, we made paired somatic recordings and applied TTX locally over the soma of one neuron, taking care to not block somatic action potentials in its coupled neighbor (**Fig. 4a**). Although the application of TTX did not completely block all somatic spikes, it revealed a large number of dendritic spikes underlying the cell's response[30,31] (**Supplementary Fig. 9**). Thus, this method enabled us to simultaneously measure light-evoked dendritic spikes from one cell and somatic action potentials from its coupled neighbor (**Fig. 4c**). Plotting cross-correlograms of pre-junctional somatic spikes and post-junctional dendritic spikes

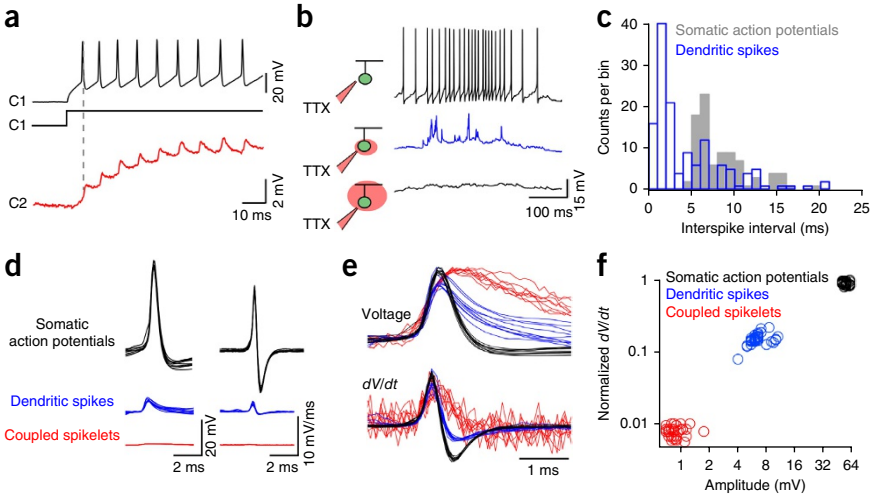

Figure 3 Gap junction inputs on their own do not trigger dendritic spikes. (**a**) Spike trains evoked in C1 (black, 200-pA depolarizing current step injected through the patch electrode) drove coupled spikelets in C2 (red), which were exclusively mediated by gap junctions (spikelets are shown on a magnified scale). (**b**) Local application of TTX blocked somatic spikes (top, black), revealing dendritic spikes (middle, blue) that were abolished when TTX was applied over the entire cell (bottom). (**c**) A plot of the interspike interval (dendritic spikes (blue) and somatic action potentials (gray), $n = 91$ action potentials and 139 dendritic spikes from 4 cells) illustrates a ~5-ms refractory period for somatic action potentials, but not dendritic spikes. (**d**) Overlays of somatic action potentials (black), dendritic spikes (blue) and coupled spikelets (red), shown on the same scale ($n = 10$ events; left). The time derivative of these events is shown on the right. (**e**) Normalized versions of the traces shown in **d**, emphasizing the different kinetics of the somatically measured events. (**f**) The maximum rate of change in voltage plotted against the peak voltage for the three types of events (35 events are plotted for each type). For this plot, light-evoked somatic action potentials and dendritic spikes were from the same cell that was hyperpolarized to increase the failure of somatic action potentials (**Supplementary Fig. 6**), whereas coupled spikelets were measured using the protocol shown in **a**.

under these conditions revealed a large increase in the probability of dendritic spikes within 2 ms of somatic action potentials in the coupled neighbor (**Fig. 4d**). In contrast, somatic action potentials did not occur shortly after dendritic spikes in coupled neighbors (although when cross-correlograms were averaged over four pairs, a weak trend started to emerge; **Supplementary Fig. 10**). These results indicate that somatic action potentials in one neuron can back-propagate, pass through gap junctions and effectively modulate the timing of dendritic spikes in coupled neighbors. Thus, fine-scale synchronization of neural activity appears to originate at the level of dendrites.

Fine-scale correlations are spatially restricted

Although coupled spikelets are relatively small at the soma because of dendritic filtering and do not effectively drive output spiking (**Fig. 2**), these electrical signals are expected to be larger near the gap junctions, where they can effectively sum with chemical synaptic inputs to drive dendritic spikes (**Fig. 4**). To determine the spatial dimensions of the dendritic trees over which electrical and chemical synaptic inputs summate, we compared the strength of correlated activity evoked using two different stimulation procedures. In the first procedure, a small spot (40–80-µm diameter) was used to locally stimulate overlapping regions of the receptive fields of neighboring cRGCs (**Fig. 5a–c**) so as

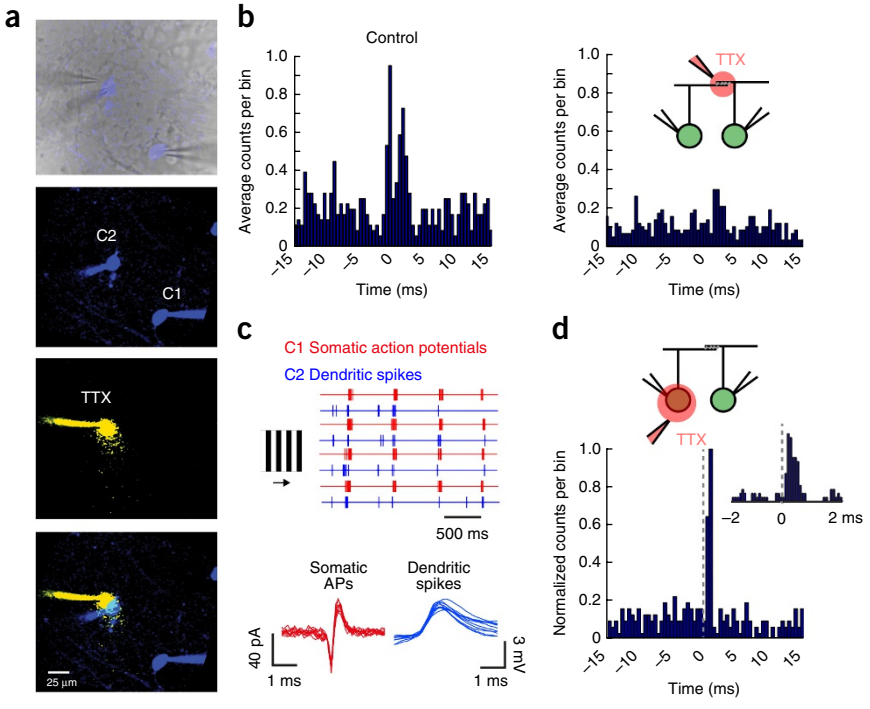

Figure 4 Dendritic spikes appear to mediate gap junction–dependent fine-scale synchronization. (**a**) Top, an infrared image depicting the recording configuration (a fluorescent image is overlaid to show *Hb9*$^+$ GFP cells in blue). The panels below show fluorescent images of the Alexa 488–filled somata of neighboring cRGCs (green channel shown in blue), the local TTX puff imaged in a separate channel (Alexa 594 was included in the puff pipette, red channel shown in yellow) and an overlay of these images. (**b**) Cross-correlograms computed for light-evoked spike trains from a pair of cRGCs in control conditions (left) and when TTX was locally applied over the region of dendritic overlap (right). (**c**) Responses to drifting gratings (top, four trials) are shown for a paired recording in which TTX was locally puffed over the soma of C2. Somatic action potentials (APs) were measured extracellularly from C1 (red traces) and dendritic spikes were measured intracellularly from C2 (blue traces; see **Supplementary Fig. 9** for experimental details). Individual extracellular spikes (C1, red) and dendritic spikes (C2, blue) are shown below at a higher resolution (ten events are shown for each). (**d**) A cross-correlogram (0.5-ms bins) plotting the distribution of dendritic spike times (measured in C2) relative to action potentials in C1 (set at time 0). The inset shows a cross-correlogram of the same events in **d**, but sampled at a higher time resolution (0.1-ms bins), illustrating that the dendritic spikes in C2 showed an increased probability of occurring shortly after a spike in C1.

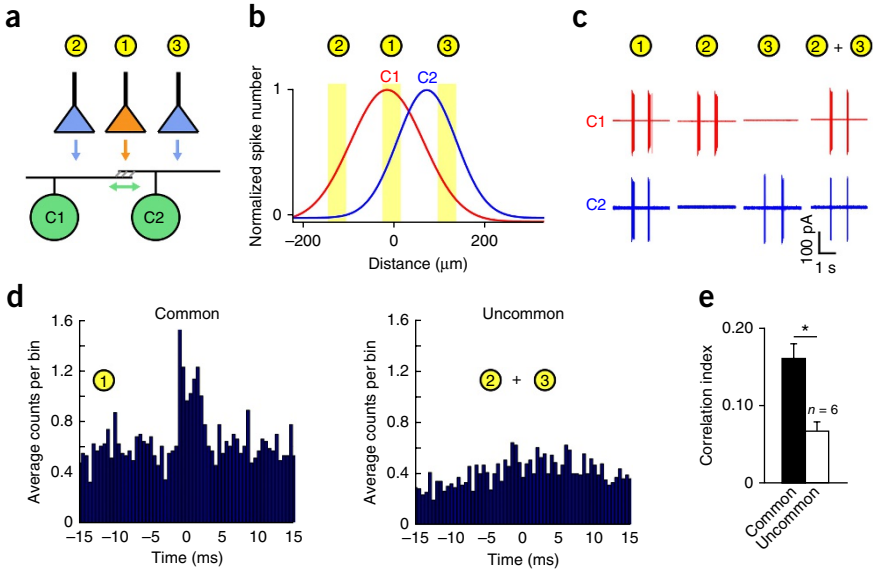

Figure 5 Gap junction–mediated correlations are spatially restricted to overlapping dendritic regions. (**a**) An illustration of the experimental protocol depicting small spot stimuli positioned to stimulate common or non-overlapping regions of the receptive fields of neighboring cRGCs. (**b**) The location of the three spots are overlaid over the experimentally measured receptive fields, estimated with one-dimensional Gaussian functions (Online Methods). (**c**) The light-evoked spiking response of the pair of neurons shown in **b** following stimulation of either common (spot 1) or uncommon regions (spot 2 + 3). (**d**) Representative cross-correlograms constructed from spike trains during stimulation of common (left) or uncommon regions (right). (**e**) The average CI values for activity driven by common and uncommon input as shown in **d**. Error bars, s.e.m.

to recruit gap junction and chemical synaptic inputs in close spatial proximity. In the second protocol, we used two spots to simultaneously stimulate flanking, non-overlapping regions of the receptive fields so that gap junction inputs and chemical synaptic inputs stimulated different regions of each cell's dendritic tree (note that each spot presented alone only activated a single cell; **Fig. 5a–c**).

Both the single and two spot procedures stimulated the pair of cRGCs to approximately the same extent (131 ± 9 Hz peak rate for common region stimulation, 115 ± 4 Hz for uncommon region stimulation; $n = 6$ pairs, $P = 0.124$, $t_5 = 1.846$, paired t test; **Supplementary Fig. 11**). Notably, although robust fine scale–correlated spike activity was observed when common regions between neighboring cells were stimulated (CI = 0.16 ± 0.03, $n = 6$ pairs), stimulation of uncommon regions resulted in significantly weaker correlations (CI = 0.07 ± 0.01, $n = 6$ pairs, $P = 0.003$, $t_5 = 5.192$, paired t test; **Fig. 5d,e**). As coupled spikelets can be measured in cRGC somata whenever a pre-junctional neighbor fires an action potential, regardless of where in its receptive field it is stimulated[13], we conclude that fine-scale synchronization only occurs when chemical and electrical synaptic inputs are activated in close spatial proximity (that is, in the overlapping region between coupled neighbors), similar to what has previously been described for medium timescale RGC correlations[34,35], which arise from shared presynaptic circuitry[12,34,35].

Correlation strength decreases with increasing firing rate

Previous work has demonstrated that correlations driven by common synaptic inputs can vary with spike rate[36,37]. Given that many of the manipulations that we have presented altered the spike rate to some extent, we next explicitly tested how three distinct manipulations that alter spike rate affect correlations. In every case, the strength of fine-scale correlations (relative to uncorrelated spikes) was inversely proportional to spike rate.

First, we modulated spike rate by changing the contrast of stimuli flashed over the receptive fields of the recorded cells. We found that reducing the spike rate by reducing contrast led to a marked increase in correlation strength

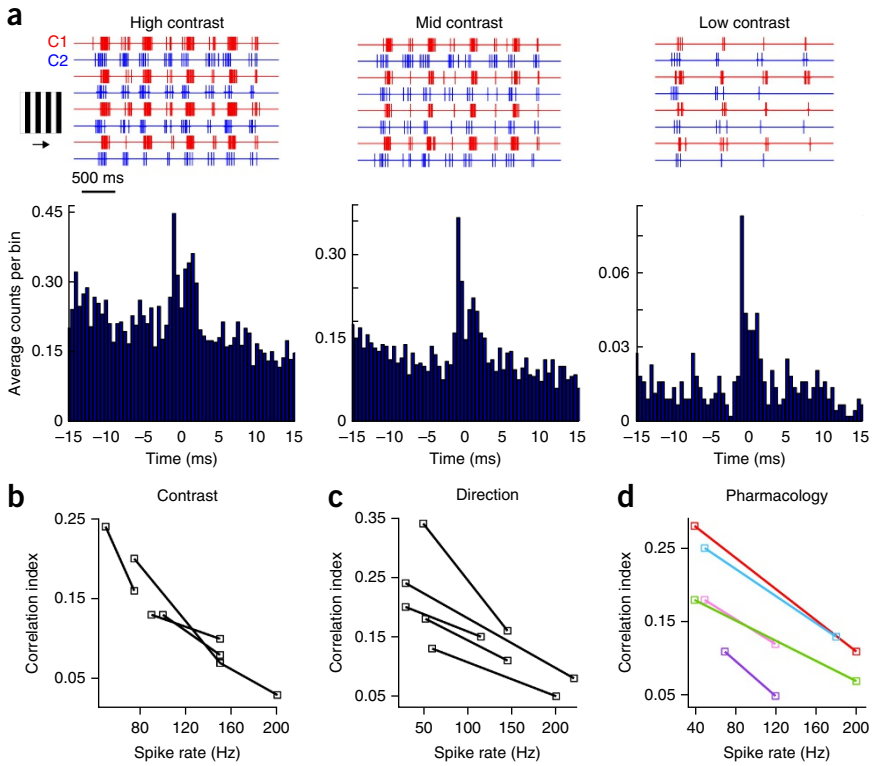

Figure 6 Correlation strength varies inversely with spike rate. (**a**) Representative spiking responses to moving gratings of high, mid and low contrast recorded from a pair of cRGCs (top, four trials are shown) from which cross-correlograms (bottom) were computed. (**b–d**) Spike rate was modulated by changing contrast, direction or using pharmacology. The average peak spike rate versus CI for individual pairs is plotted for the different conditions (as labeled). Examples in which the average peak spike rate of the two cells decreased (red = control versus 20 μM NBQX; pink = control versus 50 μM AP5; purple = control versus 50 μM tubocurare) or increased (blue = control versus 50 μM picrotoxin; green = picrotoxin high contrast versus picrotoxin low contrast) are shown in **d**.

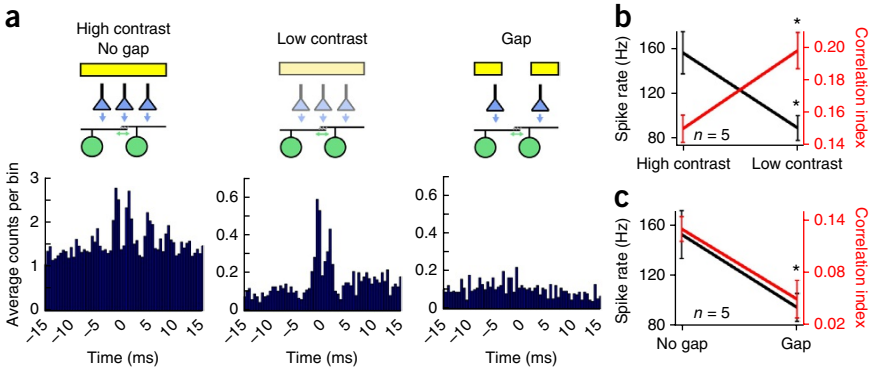

Figure 7 Correlated action potentials carry information that is independent of the spike rate. (**a**) A cross-correlogram computed from spike trains evoked by a high-contrast bar (100 × 400 µm, left), the same bar presented at lower contrast (middle) or when a gap in the stimulus was used to decrease stimulation of the overlapping regions between the pair of cRGCs (right), as indicated in the cartoon (top). Note that varying the contrast of the bar produced a similar change in the spike rate of cRGCs as changing the pattern of the stimulus. (**b**,**c**) Plots of the average peak spike rate (black) and CI (red) for responses to bars of high or low contrast and for bars without or with a gap, respectively. Error bars, s.e.m.

(high-contrast peak spike rate = 145 ± 18 Hz, low-contrast rate 93 ± 15 Hz, n = 6 pairs, P = 0.003, t_5 = 6.377, paired t test; high-contrast CI = 0.09 ± 0.02, low-contrast CI = 0.15 ± 0.03, n = 6 pairs, P = 0.022, t_5 = 3.655, paired t test; note that the CI provides a measure of the relative strength of correlated versus uncorrelated spikes, not an increase in the absolute rate of correlated spiking events; **Fig. 6a**,**b**).

Second, given that the cRGCs being studied were directionally selective, we next modulated spike rate by varying stimulus direction. Notably, stimuli moving in the null (anti-preferred) direction, despite driving far fewer action potentials than preferred direction–moving stimuli, resulted in stronger correlations (preferred direction peak spike rate = 165 ± 19 Hz, null direction rate = 45 ± 6 Hz, n = 5 pairs, P = 0.004, t_4 = 6.061, paired t test; preferred direction CI = 0.11 ± 0.02, null direction CI = 0.22 ± 0.04, n = 5 pairs, P = 0.014, t_4 = 4.160, paired t test; **Fig. 6c**). From a mechanistic standpoint, this is interesting as it indicates that gap junction signals are not simply overwhelmed by the low input resistance during large inhibitory synaptic events, such as those initiated during null direction motion[21]. However, as spiking in the null direction was not always evident on a trial-by-trial basis, we did not investigate the computational relevance of null direction correlations any further.

Third, we pharmacologically decreased the spike rate by either blocking AMPA/kainate, NMDA or acetylcholine receptors, or increased the spike rate by blocking $GABA_A$ receptors. We found that, for all pharmacological manipulations, lower spike rates were always associated with stronger correlations (excitatory blockers significantly decreased the peak rate (P = 0.003, t_5 = 5.501), but significantly increased the CI (n = 6 pairs, P = 0.004, t_5 = 4.904, paired t test pooled for different excitatory blockers); picrotoxin application increased the peak spike rate (P < 0.001; t_3 = 21.740) but decreased the CI (n = 4 pairs, P = 0.045, t_3 = 3.311, paired t test); decreasing contrast during picrotoxin application decreased the spike rate (P = 0.029, t_3 = 3.931) but increased the CI (n = 4 pairs, P = 0.011, t_3 = 5.665, paired t test); **Fig. 6**). Together, these results provide compelling evidence that the strength of gap junction–mediated correlations decreases with increasing spike rate and that no specific chemical synaptic receptors are required for driving correlations.

Correlations encode information absent from the spike rate

Finally, having gained a detailed understanding of the unique properties of gap junction–mediated correlations, we next tested the possibility that specific visual features might be differentially coded by correlations and spike rate. In particular, we considered whether the correlations carried by spike trains of cRGCs could allow for discrimination between changes in stimulus contrast versus changes in the spatial structure of stimuli within their receptive fields (**Fig. 7a**).

As expected, for a bar of light that stimulated a pair of cells, either decreasing contrast or introducing large gaps in the stimulus both led to a similar decline in the spike rate of cRGCs (peak spike rate = 157 ± 17 Hz for high contrast and 90 ± 19 Hz for low contrast, n = 5 pairs, P < 0.001, t_4 = 10.196, paired t test; peak spike rate = 153 ± 19 Hz for no gap and 95 ± 11 Hz for a large gap, n = 5 pairs, P = 0.045, t_4 = 2.878, paired t test; **Fig. 7**). However, these stimuli had opposing effects on correlations. Reducing the contrast of the stimulus significantly enhanced fine-scale correlations (CI = 0.15 ± 0.01 for high contrast and 0.20 ± 0.01 for low contrast, n = 5 pairs, P = 0.005, t_4 = 5.580, paired t test; **Fig. 7a**,**b**), whereas introducing gaps in the stimulus, and removing input to the overlapping regions between neighboring receptive fields, significantly reduced correlations (CI = 0.13 ± 0.01 for no gap and 0.05 ± 0.02 for a large gap, n = 5 pairs, P = 0.018, t_4 = 3.858, paired t test; **Fig. 7a**,**c**). Thus, it appears that gap junctions can mediate a correlation code that is complementary to the spike rate code (**Fig. 7b**,**c**) and that each code may be optimized for detecting different aspects of the visual scene.

DISCUSSION

Our results reveal that nonlinear integration of temporally coincident electrical and chemical synaptic inputs in regions of dendritic overlap between neighboring cells underlies a fine-scale synchrony code. This active dendritic mechanism produces correlations that decrease in strength as spike rate increases, forming the basis of a coding scheme that conveys information embedded in distinct dendritic arbours of coupled neurons.

Nonlinear dendritic integration underlies synchrony

Previously, it has been suggested that gap junction inputs between retinal ganglion cells could directly drive action potentials in neighboring neurons, providing a simple mechanism for creating spike synchrony[25]. However, as in other parts of the CNS[1,2], gap junctions between ganglion cells are relatively weak, and on their own do not effectively drive action potentials in coupled neighboring cells[13,14,24] (**Fig. 3a**). In his seminal work, Mastronarde observed that fine-scale spike correlations between neighboring ganglion cells appeared to be enhanced when cells received common chemical synaptic input[24], consistent with our findings here. Thus, to be effective in driving synchrony, it appears that gap junction signals must interact with chemical synaptic inputs on fine timescales.

Mechanistically, we found that electrical and chemical synaptic interactions occur through a sequence of events in which gap junction inputs initially driven by back-propagating action potentials in pre-junctional cells sum with temporally and spatially coincident chemical synaptic inputs in post-junctional cells to trigger dendritic spikes. In this scenario, gap junction–mediated inputs can interact with chemical synaptic inputs near any number of dendritic gap junction–containing sites in a certain spatial and temporal window, set by the length and

time constants of the dendrites. Dendritic spikes in turn actively propagate with little delay to the soma, where they drive action potentials with high fidelity[30,31], thereby allowing weak distal gap junction inputs to exert substantial control on the timing of somatic action potentials. Although this mechanism is reminiscent of nonlinear interactions between coincident back-propagating action potentials and NMDA receptor–mediated inputs required for driving synaptic plasticity in cortical neurons[38], the mechanisms that drive synchrony in cRGCs did not appear to drive plasticity nor did they appear to critically rely on NMDA receptors (that is, robust correlations were measured when NMDA receptors were pharmacologically blocked; **Fig. 6d**).

The finding that fine-scale correlations are resistant to blockade of chemical synaptic transmission in the salamander retina[20] seems at odds with our current model invoking nonlinear dendritic integration of electrical and chemical synapses. However, in that study, the authors noted that the net effect of blocking synaptic transmission was excitatory, raising the spontaneous firing rate of most ganglion cells[20]. Consistent with these findings, when pairs of *Hb9*$^{+}$ (also known as *Mnx1*) cRGCs were artificially depolarized through the patch electrode, robust synchrony was observed in the absence of chemical synaptic transmission (note that directionally selective ganglion cells exhibit very low spike rates in the absence of modulated light). However, under physiological conditions, gap junction–mediated spikelets at the soma were clearly ineffective at synchronizing activity. This is best evidenced in our two-spot experiment (**Fig. 5**), where non-overlapping regions of the receptive fields were used to simultaneously depolarize neighboring cells. Although the somata of both cells were brought near threshold, coupled spikelets failed to synchronize activity. Notably, the same pair of cells could subsequently be synchronized using a single spot placed in between them that activated chemical and electrical synapses in close spatial proximity. These results strongly support the idea that nonlinear integration of temporally and spatially coincident electrical and chemical synaptic inputs is a prerequisite for synchrony under natural conditions.

Correlation strength was found to vary inversely with spike rate. Although this property appears to be consistent with findings for other gap junction–coupled neurons[39,40], it sharply contrasts with synchrony generated by common input measured in other parts of the brain, where output correlations are found to increase with spike rate[36,37]. Correlations driven by common input are generally found to be weak at low spike rates because they are masked by the spike threshold and therefore only become evident at higher activity levels[36,37]. In contrast, in gap junction–coupled neurons, during periods of low activity, a single pre-junctional action potential generates a near synchronous electrical input in post-junctional cells, which can in turn nonlinearly sum with chemical synaptic inputs at any one of a large number of dendritic sites (on average there are ~50–100 possible electrical synapses, as determined by the number of dendritic crossings between pairs of cRGCs; data not shown). Thus, gap junction inputs are often the determining factor of whether a cell reaches spike threshold or not, resulting in strong synchrony during periods of low spike activity. However, during periods of high spike activity (peak spike rates ~250–300 Hz), large voltage-dependent and chemical synaptic conductances dominate the dendritic membrane potential and likely attenuate the effect of gap junction inputs. Together, the properties that we describe distinguish gap junction–mediated correlations from common input mediated correlations and suggest that both correlation types may have different consequences for neural encoding.

Aside from generating correlated firing, we have previously shown that gap junction signals cooperate with chemical synapses to provide strong lateral anticipatory signals allowing these motion-coding cRGCs to begin responding to the edges of moving objects before they enter the classic receptive field[14]. These gap junction–mediated anticipatory signals, however, differ from gap junction–mediated synchronization signals in several respects. First, although synchronization signals appear to be derived from individual action potentials, anticipatory signals are derived primarily from the slow global EPSPs of upstream cells and are further compounded through a population effect[14]. Second, synchronization signals operate throughout the light-evoked response, whereas anticipatory signals are most effective at the onset of the response when the cell is not strongly activated by chemical synaptic conductances, such that leading-edge gap junction inputs help to push a cell more quickly past spike threshold, thereby compensating for delays in photoreceptor signal transduction. Lastly, anticipatory signals are extremely sensitive to activity-dependent spike adaptation in coupled neurons and are therefore invoked most effectively by the leading edges of isolated stimuli moving on a featureless background[13]. In contrast, synchronization signals are effective throughout continuous bouts of activity, as when stimulated by drifting gratings (~1–2-Hz temporal frequency). Thus, gap junctions can have distinct computational roles depending on the stimulus conditions.

Fine-scale synchrony and direction encoding

Here we demonstrated a form of spike correlation that differs from medium timescale correlations, similar to those generated by common input, in both underlying mechanism and statistical properties. Do the unique properties of this fine-scale synchronous activity confer an advantage to cRGCs in direction encoding? Definitively answering this question requires a more thorough theoretical framework than is possible in the scope of this study, but below we outline some possible roles for these fine-scale correlations.

Our findings, coupled with previous work on retino-geniculate circuitry in mouse, cat and primate, suggest that synchronous activity may improve the ability of cRGCs to transmit information about the direction of motion of visual stimuli under diverse stimulus conditions. In the mouse, directionally selective neurons in the lateral geniculate nucleus (LGN) appear to inherit their response properties directly from directionally selective RGCs[41]. In addition, individual LGN neurons receive converging input from ~1–3 RGCs[42], likely arising from the same class of cells[43]. Given that nonlinear summation of near-coincident inputs greatly increases the efficacy of retino-geniculate synapses[44,45], it is likely that the rapid synchronous firing events described here would be especially effective at driving LGN neurons receiving converging inputs from neighboring cRGCs. Furthermore, the inverse spike rate-correlation relationship displayed by cRGCs means that, under conditions in which cRGCs are only weakly driven, synchronous activity will be particularly important. Nonlinear summation of synchronous inputs by LGN neurons could ensure that cRGCs reliably convey information even during suboptimal stimulation. A prediction would be that directional-selective LGN neurons that receive input from cRGCs will maintain robust direction selectivity over a wider range of stimulus conditions than LGN neurons coding other directions (as directionally selective RGCs coding other directions are not gap junction coupled in the mature retina[13]). Moreover, given the prevalence of dendritic electrical coupling[3–11] and active dendritic properties[46–49] in neural circuits throughout the CNS, it is likely that mechanisms similar to those presented here may be a general solution to the problem of reliably transmitting weak signals in noisy neural systems.

Finally, correlated activity between groups of neurons may either limit or increase the accuracy of neural coding depending on the

precise structure of correlations (for a review see ref. 50). In the retina, it has been proposed that visual information could be encoded by synchronous spike activity itself[34,35]. We found that the spike activity of pairs of cRGCs could transmit information about the spatial location of a visual stimulus independent of other parameters that modulate spike rate, such as contrast. However, whether and how this information is used by downstream circuits remains a challenge for future work.

METHODS

Methods and any associated references are available in the online version of the paper.

Note: Any Supplementary Information and Source Data files are available in the online version of the paper.

ACKNOWLEDGMENTS

We thank K. Delaney, A. Pereda and S. Sethuramanujam for their helpful comments on this manuscript, D. Paul for kindly providing the *Cx36*$^{-/-}$ mice, J. Boyd (University of British Columbia) for his help in writing software for two-photon imaging, and A. Sullivan for maintaining mouse colonies. This work was supported by US National Institutes of Health grants R01-EY022070 (R.G.S.) and R01-EY11850 (F.R.), National Eye Institute grant EY07031 (M.H.T.), the Howard Hughes Medical Institute (F.R.), and by the Canadian Institutes of Health Research (130268-2013, G.B.A.) and Foundation for Fighting Blindness (Canada, G.B.A.).

AUTHOR CONTRIBUTIONS

This study was designed by S.T., D.J.S., A.J.M., F.R., M.H.T. and G.B.A. All of the experiments were performed by S.T. and A.J.M. (except for those presented in **Fig. 2d–f**, which were performed by M.H.T.). The results were analyzed by S.T., A.J.M., M.H.T. and D.J.S. The paper was written by S.T., D.J.S., M.H.T., F.R., R.G.S. and G.B.A.

COMPETING FINANCIAL INTERESTS

The authors declare no competing financial interests.

1. Connors, B.W. & Long, M.A. Electrical synapses in the mammalian brain. *Annu. Rev. Neurosci.* **27**, 393–418 (2004).
2. Bennett, M.V. & Zukin, R.S. Electrical coupling and neuronal synchronization in the mammalian brain. *Neuron* **41**, 495–511 (2004).
3. Hidaka, S., Akahori, Y. & Kurosawa, Y. Dendrodendritic electrical synapses between mammalian retinal ganglion cells. *J. Neurosci.* **24**, 10553–10567 (2004).
4. Fukuda, T. & Kosaka, T. Ultrastructural study of gap junctions between dendrites of parvalbumin-containing GABAergic neurons in various neocortical areas of the adult rat. *Neuroscience* **120**, 5–20 (2003).
5. Sotelo, C., Llinas, R. & Baker, R. Structural study of inferior olivary nucleus of the cat: morphological correlates of electrotonic coupling. *J. Neurophysiol.* **37**, 541–559 (1974).
6. Fukuda, T. & Kosaka, T. Gap junctions linking the dendritic network of GABAergic interneurons in the hippocampus. *J. Neurosci.* **20**, 1519–1528 (2000).
7. Ishimatsu, M. & Williams, J.T. Synchronous activity in locus coeruleus results from dendritic interactions in pericoerulear regions. *J. Neurosci.* **16**, 5196–5204 (1996).
8. Wouterlood, F.G., Mugnaini, E., Osen, K.K. & Dahl, A.L. Stellate neurons in rat dorsal cochlear nucleus studies with combined Golgi impregnation and electron microscopy: synaptic connections and mutual coupling by gap junctions. *J. Neurocytol.* **13**, 639–664 (1984).
9. Schoppa, N.E. & Westbrook, G.L. AMPA autoreceptors drive correlated spiking in olfactory bulb glomeruli. *Nat. Neurosci.* **5**, 1194–1202 (2002).
10. Vervaeke, K. *et al.* Rapid desynchronization of an electrically coupled interneuron network with sparse excitatory synaptic input. *Neuron* **67**, 435–451 (2010).
11. Dugué, G.P. *et al.* Electrical coupling mediates tunable low-frequency oscillations and resonance in the cerebellar Golgi cell network. *Neuron* **61**, 126–139 (2009).
12. Trong, P.K. & Rieke, F. Origin of correlated activity between parasol retinal ganglion cells. *Nat. Neurosci.* **11**, 1343–1351 (2008).
13. Trenholm, S., McLaughlin, A.J., Schwab, D.J. & Awatramani, G.B. Dynamic tuning of electrical and chemical synaptic transmission in a network of motion coding retinal neurons. *J. Neurosci.* **33**, 14927–14938 (2013).
14. Trenholm, S., Schwab, D.J., Balasubramanian, V. & Awatramani, G.B. Lag normalization in an electrically coupled neural network. *Nat. Neurosci.* **16**, 154–156 (2013).
15. Vervaeke, K., Lorincz, A., Nusser, Z. & Silver, R.A. Gap junctions compensate for sublinear dendritic integration in an inhibitory network. *Science* **335**, 1624–1628 (2012).
16. Mathy, A., Clark, B.A. & Hausser, M. Synaptically induced long-term modulation of electrical coupling in the inferior olive. *Neuron* **81**, 1290–1296 (2014).
17. Lefler, Y., Yarom, Y. & Uusisaari, M.Y. Cerebellar inhibitory input to the inferior olive decreases electrical coupling and blocks subthreshold oscillations. *Neuron* **81**, 1389–1400 (2014).
18. Turecek, J. *et al.* NMDA receptor activation strengthens weak electrical coupling in mammalian brain. *Neuron* **81**, 1375–1388 (2014).
19. Migliore, M., Hines, M.L. & Shepherd, G.M. The role of distal dendritic gap junctions in synchronization of mitral cell axonal output. *J. Comput. Neurosci.* **18**, 151–161 (2005).
20. Brivanlou, I.H., Warland, D.K. & Meister, M. Mechanisms of concerted firing among retinal ganglion cells. *Neuron* **20**, 527–539 (1998).
21. Trenholm, S., Johnson, K., Li, X., Smith, R.G. & Awatramani, G.B. Parallel mechanisms encode direction in the retina. *Neuron* **71**, 683–694 (2011).
22. Shlens, J., Rieke, F. & Chichilnisky, E. Synchronized firing in the retina. *Curr. Opin. Neurobiol.* **18**, 396–402 (2008).
23. Mastronarde, D.N. Correlated firing of retinal ganglion cells. *Trends Neurosci.* **12**, 75–80 (1989).
24. Mastronarde, D.N. Interactions between ganglion cells in cat retina. *J. Neurophysiol.* **49**, 350–365 (1983).
25. Hu, E.H. & Bloomfield, S.A. Gap junctional coupling underlies the short-latency spike synchrony of retinal alpha ganglion cells. *J. Neurosci.* **23**, 6768–6777 (2003).
26. DeVries, S.H. Correlated firing in rabbit retinal ganglion cells. *J. Neurophysiol.* **81**, 908–920 (1999).
27. Völgyi, B. *et al.* Gap junctions are essential for generating the correlated spike activity of neighboring retinal ganglion cells. *PLoS ONE* **8**, e69426 (2013).
28. Trenholm, S. *et al.* Intrinsic oscillatory activity arising within the electrically coupled AII amacrine-ON cone bipolar cell network is driven by voltage-gated Na^+ channels. *J. Physiol. (Lond.)* **590**, 2501–2517 (2012).
29. Mann-Metzer, P. & Yarom, Y. Electrotonic coupling interacts with intrinsic properties to generate synchronized activity in cerebellar networks of inhibitory interneurons. *J. Neurosci.* **19**, 3298–3306 (1999).
30. Sivyer, B. & Williams, S.R. Direction selectivity is computed by active dendritic integration in retinal ganglion cells. *Nat. Neurosci.* **16**, 1848–1856 (2013).
31. Oesch, N., Euler, T. & Taylor, W.R. Direction-selective dendritic action potentials in rabbit retina. *Neuron* **47**, 739–750 (2005).
32. Curti, S., Hoge, G., Nagy, J.I. & Pereda, A.E. Synergy between electrical coupling and membrane properties promotes strong synchronization of neurons of the mesencephalic trigeminal nucleus. *J. Neurosci.* **32**, 4341–4359 (2012).
33. Haas, J.S. & Landisman, C.E. State-dependent modulation of gap junction signaling by the persistent sodium current. *Front. Cell. Neurosci.* **5**, 31 (2011).
34. Meister, M., Lagnado, L. & Baylor, D.A. Concerted signaling by retinal ganglion cells. *Science* **270**, 1207–1210 (1995).
35. Schnitzer, M.J. & Meister, M. Multineuronal firing patterns in the signal from eye to brain. *Neuron* **37**, 499–511 (2003).
36. de la Rocha, J., Doiron, B., Shea-Brown, E., Josic, K. & Reyes, A. Correlation between neural spike trains increases with firing rate. *Nature* **448**, 802–806 (2007).
37. Litwin-Kumar, A., Oswald, A.M., Urban, N.N. & Doiron, B. Balanced synaptic input shapes the correlation between neural spike trains. *PLoS Comput. Biol.* **7**, e1002305 (2011).
38. Larkum, M.E., Zhu, J.J. & Sakmann, B. A new cellular mechanism for coupling inputs arriving at different cortical layers. *Nature* **398**, 338–341 (1999).
39. Alvarez, V.A., Chow, C.C., Van Bockstaele, E.J. & Williams, J.T. Frequency-dependent synchrony in locus ceruleus: role of electrotonic coupling. *Proc. Natl. Acad. Sci. USA* **99**, 4032–4036 (2002).
40. Xiao, L., Zhang, M., Xing, D., Liang, P.J. & Wu, S. Shifted encoding strategy in retinal luminance adaptation: from firing rate to neural correlation. *J. Neurophysiol.* **110**, 1793–1803 (2013).
41. Piscopo, D.M., El-Danaf, R.N., Huberman, A.D. & Niell, C.M. Diverse visual features encoded in mouse lateral geniculate nucleus. *J. Neurosci.* **33**, 4642–4656 (2013).
42. Chen, C. & Regehr, W.G. Developmental remodeling of the retinogeniculate synapse. *Neuron* **28**, 955–966 (2000).
43. Cleland, B.G., Dubin, M.W. & Levick, W.R. Simultaneous recording of input and output of lateral geniculate neurones. *Nat. New Biol.* **231**, 191–192 (1971).
44. Carandini, M., Horton, J.C. & Sincich, L.C. Thalamic filtering of retinal spike trains by postsynaptic summation. *J. Vis.* **7**, 20.1–20.11 (2007).
45. Usrey, W.M., Reppas, J.B. & Reid, R.C. Paired-spike interactions and synaptic efficacy of retinal inputs to the thalamus. *Nature* **395**, 384–387 (1998).
46. Chiovini, B. *et al.* Dendritic spikes induce ripples in parvalbumin interneurons during hippocampal sharp waves. *Neuron* **82**, 908–924 (2014).
47. Smith, S.L., Smith, I.T., Branco, T. & Hausser, M. Dendritic spikes enhance stimulus selectivity in cortical neurons *in vivo*. *Nature* **503**, 115–120 (2013).
48. Palmer, L.M. *et al.* NMDA spikes enhance action potential generation during sensory input. *Nat. Neurosci.* **17**, 383–390 (2014).
49. Grienberger, C., Chen, X. & Konnerth, A. NMDA receptor-dependent multidendrite Ca^{2+} spikes required for hippocampal burst firing *in vivo*. *Neuron* **81**, 1274–1281 (2014).
50. Shamir, M. Emerging principles of population coding: in search for the neural code. *Curr. Opin. Neurobiol.* **25**, 140–148 (2014).

ONLINE METHODS

Whole-mount retinal preparation. All procedures were either performed in accordance with the Canadian Council on Animal Care and approved by the University of Victoria's Animal Care Committee or were approved by the University of Washington's Animal Care Committee. Experiments were performed with adult *Hb9::eGFP* transgenic mice[21], C57Bl/6 mice (wild type) or *Cx36*$^{-/-}$ mice (kindly provided by D. Paul, Harvard University) of either sex that were maintained on a 12-h light/dark cycle. In short, mice were dark-adapted for approximately 30–60 min before being anesthetized and decapitated. The retina was dissected in Ringer's solution under infrared light. The isolated retina was then mounted on a 0.22-mm membrane filter (Millipore) with a pre-cut window to allow light to reach the retina and enabling the preparation to be viewed with infrared light using a Spot RT3 CCD camera (Diagnostic Instruments) attached to an upright Olympus BX51 WI fluorescent microscope outfitted with a 40× water-immersion lens (Olympus Canada). The isolated retina was then perfused with heated Ringer's solution (35–37 °C) containing 110 mM NaCl, 2.5 mM KCl, 1 mM $CaCl_2$, 1.6 mM $MgCl_2$, 10 mM dextrose and 22 mM $NaHCO_3$ that was bubbled with carbogen (95% O_2:5% CO_2). Unless otherwise noted, all reagents were purchased form Sigma-Aldrich Canada.

Physiological recordings. Spike recordings were made using the loose cell-attached patch-clamp technique using 5–10-MΩ electrodes filled with Ringer's solution. For current-clamp experiments, 5–8-MΩ electrodes contained 115 mM potassium gluconate, 9.7 mM KCl, 1 mM $MgCl_2$, 0.5 mM $CaCl_2$, 1.5 mM EGTA, 10 mM HEPES, 4 mM ATP-Mg_2, 0.5 mM GTP-Na_3, 0.025 mM Alexa 594 and 7.75 mM Neurobiotin. The pH was adjusted to 7.2–7.3 with KOH. Recordings were made with a MultiClamp 700B amplifier (Molecular Devices). Signals were digitized at 10 kHz (PCI-6036E acquisition board, National Instruments) and acquired using custom software written in LabVIEW. GFP$^+$ ganglion cells were visually targeted for recordings using two-photon laser-scanning microscopy techniques with the wavelength at 920 nm to minimize photoreceptor bleaching. GFP$^-$ DSGCs were identified by their medium-sized elliptical somata and their ON-OFF directionally selective response properties that differed in preferred direction from *Hb9*$^+$ cells. For experiments in which spikelets were simulated with current injection (**Fig. 2d–f**), after ON-OFF DSGCs were identified, a whole-cell recording was made using a 3–6-M electrode containing 125 mM potassium aspartate, 1 mM $MgCl_2$, 10 mM KCl, 10 mM HEPES, 2 mM EGTA, 1 mM $CaCl_2$, 4 mM ATP and 0.5 mM GTP, pH 7.2 with KOH. In these experiments, in some cases to compensate for an offset introduced after making a whole-cell recording, a small amount of hyperpolarizing current was injected throughout the recording to help maintain the low spontaneous spike rate and robust light responses typical of ON-OFF DS cells seen in the loose-patch configuration. For TTX puff experiments, 1 µM TTX was included in a recording electrode and positive pressure was applied to locally puff TTX.

Light stimulus. Light stimuli were produced via a digital projector (Hitachi Cpx1, refresh rate 75 Hz) or with an OLED monitor (eMagin) that was controlled with custom-written software incorporating Psychtoolbox. The ambient background intensity, measured with a calibrated spectrophotometer (USB2000, Ocean Optics), was set to approximately ~500 to 1000 R* per rod per s. Light stimuli, projected from below the preparation, were focused with the substage condenser onto the outer segments of the photoreceptors.

Cross-correlograms and correlation index. Cross-correlograms were computed from spike trains measured in neighboring cRGCs, evoked by static flashes, moving bars or moving gratings (usually 50–400 repetitions or cycles). Cross-correlograms were constructed on the basis of the relative time differences between spikes observed in neighboring neurons C1 and C2 (that is, using the spike train from C1 as the reference and spikes from C2 to make the histogram). Relative spike times were parsed into 0.5-ms bins (unless otherwise noted) and the correlograms were averaged over multiple trials. To estimate stimulus driven correlations, we re-computed cross-correlograms after shuffling trials using conventional methods, thereby obtaining a 'shift predictor' (**Supplementary Fig. 1**). However, for all text figures, cross-correlograms were not shift predicted, to allow an assessment of stimulus driven activity under different experimental conditions.

To quantify correlations, we calculated a CI. To do so, we first discretized time into 4-ms bins (to capture the peaks of the cross-correlogram) and assigned the value 1 to a bin if the neuron spiked within it and 0 otherwise. We then computed the Pearson correlation coefficient (CC) between spike trains in the two neurons (where spike covariance of the two neurons is normalized by the geometric variance of their firing rates[36]). To remove stimulus driven correlations, we computed the CC on a shuffled set of trials (SCC) and then defined the CI as CC – SCC.

Simulated spikelet injections. Ten different spikelet patterns were generated using a 20-Hz Poisson spike generator to randomly assign spikelet times. The spikelet waveform used was the peak-aligned average of ~100 spikelet currents measured in voltage-clamp from a coupled ON-OFF DS cell (data not shown). While injecting a Poisson-generated spikelet pattern into a cell, a 300-µm bright square was flashed for 1 s over the cell's receptive field. The amplitude of the injected spikelets was controlled by scaling the entire waveform by a constant factor. The depolarization induced by each spikelet was defined as the maximum membrane potential in a 13-ms window surrounding an injected spikelet time. Depolarizations in that window that surpassed spike threshold were not considered. For each of five to six spikelet amplitudes, roughly 3,000 spikelets were injected over 60 trials for each cell. As with spike trains, cross-correlograms between binarized spike and spikelet trains were constructed. Cross-correlograms were normalized by the geometric mean of the spike and spikelet autocorrelation functions to yield a correlation value as a function of time delay (**Fig. 2f**).

Directional selectivity index. To calculate the preferred direction for directionally selective ganglion cells (DSGCs), a vector sum was computed from the peak spike rates produced by presenting a 300 × 300 µm (96% positive Weber contrast = difference in luminance between foreground and background/average background luminance) stimuli moving at 600 µm s^{-1} in eight directions over each cell. The strength of directional selectivity was calculated with a direction selectivity index (DSI) that was measured as the peak spike rate in the preferred direction (P) minus the peak spike rate in the null direction (N), divided by the sum of these two rates: (P – N / P + N). The length of the preferred direction vector plotted on the polar plot was a normalized representation of DSI. Gaussian receptive fields were calculated by marching a small white spot (40–80-µm diameter) over a cell along a single axis, plotting the peak spike rate for each spatial location and then fitting these points with a single Gaussian function (note, these cells do not have a conventional antagonistic surround receptive field[13]).

Data analysis. Comparisons between groups were made with *t* tests. Comparisons made between recordings from the same cell before and after applying pharmacological agents (or before and after experimental manipulation, such as changing the contrast) were made using paired *t* tests. For comparison between multiple groups, we used a one-way ANOVA. Data are presented as mean ± s.e.m. All data used for analysis with *t* tests and paired *t* tests were tested for normality using the Shapiro-Wilk normality test and passed the test. The data for the ANOVA failed the normality test, so we used the Kruskal-Wallis one-way ANOVA on ranks.

A **Supplementary Methods Checklist** is available.